Nanotopography Modulates Mechanotransduction of Stem Cells and Induces Differentiation through Focal Adhesion Kinase

Benjamin Kim Kiat Teo,[†,‡] Sum Thai Wong,[†,§] Choon Kiat Lim,[‡] Terrence Y. S. Kung,[‡] Chong Hao Yap,[‡] Yamini Ramagopal,[‡] Lewis H. Romer,[⊥] and Evelyn K. F. Yim[†,‡,∥,*]

[†]Department of Bioengineering, National University of Singapore, 9 Engineering Drive 1, EA 03-12, Singapore 117576, Singapore, [‡]Mechanobiology Institute Singapore, National University of Singapore, T-Lab, #05-01, 5A Engineering Drive 1, Singapore 117411, Singapore, [§]Institute of High Performance Computing, A*STAR, Singapore, 1 Fusionopolis Way, #16-16 Connexis, Singapore 138632, Singapore, [⊥]Departments of Anesthesiology and Critical Care Medicine, Cell Biology, Biomedical Engineering, Pediatrics, and the Center for Cell Dynamics, Johns Hopkins University School of Medicine, Bloomberg Children's Center, Pediatric ACCM, 1800 Orleans Street, Baltimore, Maryland 21287-4904, United States, and [∥]Department of Surgery, National University of Singapore, NUHS Tower Block, Level 8, 1E Kent Ridge Road, Singapore 119228, Singapore

ABSTRACT Regulated biophysical cues, such as nanotopography, have been shown to be integral for tissue regeneration and embryogenesis in the stem cell niche. Tissue homeostasis involves the interaction of multipotent cells with nanoscaled topographical features in their ECM to regulate aspects of cell behavior. Synthetic nanostructures can drive specific cell differentiation, but the sensing mechanisms for nanocues remain poorly understood. Here, we report that nanotopography-induced human mesenchymal stem cell (hMSC) differentiation through cell mechanotransduction is modulated by the integrin-activated focal adhesion kinase (FAK). On nanogratings with 250 nm line width on polydimethylsiloxane, hMSCs developed aligned stress fibers and showed an upregulation of neurogenic and myogenic differentiation markers. The observed cellular focal adhesions within these cells were also significantly smaller and more elongated on the nanogratings compared to microgratings or unpatterned control. In addition, our mechanistic study confirmed that this regulation was dependent upon actomyosin contractility, suggesting a direct force-dependent mechanism. The topography-induced differentiation was observed on different ECM compositions but the response was not indicative of a direct ECM-induced hMSC differentiation pathway. FAK phosphorylation was required for topography-induced hMSC differentiation while FAK overexpression overruled the topographical cues in determining cell lineage bias. The results indicated that FAK activity had a direct impact on topography-induced gene expression, and that this effect of FAK was independent of cell shape. These findings suggest that hMSC sense and transduce nanotopographical signals through focal adhesions and actomyosin cytoskeleton contractility to induce differential gene expression.

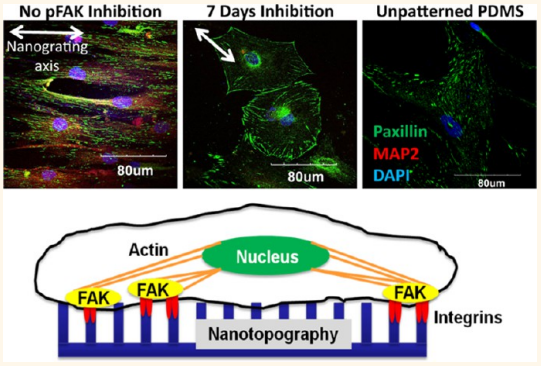

KEYWORDS: mesenchymal stem cell · cell signaling · FAK · nanotopography · differentiation · focal adhesions · physical cues

The process of tissue development involves multipotent cells that interact with various nanoscaled topographical and biochemical cues in their extracellular matrix (ECM) environment.[1] Physical cues in the form of both micro- and nanoscale topographical structures have been shown to affect various cell responses including proliferation, migration, endocytosis and differentiation.[2−4] This has spurred research efforts to be directed toward understanding the response of multipotent stem cells[5] to nanoscale features. While topographical cues have been accepted to be regulators of cell fate, the mechanism behind topography-induced cellular response has however remained unclear.

Cellular mechanical forces and its interaction with the ECM have begun to emerge as key determinants of cell behavior.[6,7] In a recent study, it was shown that geometric features that increase actomyosin contractility in hMSCs promoted osteogenesis.[8] Our earlier studies using nanogratings induced

* Address correspondence to eyim@nus.edu.sg.

Received for review October 25, 2012 and accepted May 13, 2013.

Published online May 13, 2013
10.1021/nn304966z

the differentiation of human mesenchymal stem cells (hMSCs) into the neuronal lineage.[9] In addition, hMSCs were able to sense intricate differences in feature size, showing a more significant upregulation of neuronal markers on nanogratings compared to microgratings. The understanding of topography-induced differentiation mechanism in hMSCs will be important to determine the crucial parameters of stem cell fate regulation. We hypothesize that topography-induced cell behavior is caused by a change in focal adhesion (FA) arrangement, leading to a change in the actin cytoskeleton (CSK) and mechanotransduction of the cells, resulting in differential gene expression and cell function.

In the absence of soluble differentiation factors, the signals from physical cues can be sensed by the hMSCs and translated to an upregulation of markers specific to neuronal or myogenic differentiation.[10] One possible mode of this signal transmission is mechanotransduction where physical cues are transduced *via* mechanical forces to signaling pathways involved in detecting and responding to the ECM. This interaction is initiated at the cell-matrix interface, possibly through the integrins[11] before mechanical forces exerted by the ECM are sensed by the FA complex and in turn activates downstream FA signaling pathways. FAs are multicomponent macroassemblies of protein complexes that serve as a nexus between the actin CSK and the ECM. One such protein tyrosine kinase, focal adhesion kinase (FAK), has been shown to be an important mediator in the mechanotransduction pathway by responding to both substrate rigidity and regulating tension *via* the actin CSK (reviewed in Burridge *et al.*[12]). In addition, FAK also mediates other pathways. One example includes the small GTPase RhoA. RhoA stimulates actomyosin contraction,[13] regulates cell proliferation[14] and is shown to regulate cell fate.[6] FAK may be an important regulator for cells to detect and sense the topographical features in the ECM. In order to uncover the mechanism for topography-induced cell differentiation, we aim to understand the role of FAK in the topography-induced cell differentiation. In this paper, we seek to understand the ECM's contribution to topography-induced differentiation, and the roles of intracellular contractility and FAK phosphorylation in the transduction of nanotopographical cues and in the differentiation of stem cells.

RESULTS

Nanotopography-Induced Alignment, Elongation, and Differentiation of hMSC through Modulation of Actomyosin Contractility. Polydimethylsiloxane (PDMS) nanogratings were fabricated using an established robust soft lithography protocol using a nanoimprinted poly (methyl methacrylate) (PMMA) on silicon master mold. The nanogratings were replicated on PDMS with good fidelity as shown by the scanning electron micrographs (Figure 1A). HMSCs were cultured for one week on polydimethylsiloxane (PDMS) nanogratings of 250 nm width fabricated using soft lithography. These hMSCs had aligned F-actin fiber bundles and the cells elongated along the long axis of the nanogratings. In contrast, cells on unpatterned controls showed dense, isotropic fibrous F-actin networks (Figure 1B). The topographical influence on CSK suggests a direct dependence of hMSCs differentiation on cytoskeletal force contractility. To determine if the process was dependent on nonmuscle myosin (NM II) contractility, hMSCs' cytoskeletal contractility was directly inhibited by adding the small molecule Blebbistatin (Bleb, 50 μM) into the growth media. We then quantified changes in cell shape by considering cells to be aligned when the angle between the long axis of the cell and the grating was less than 15.00°, while using the elongation parameter (Long Axis/Short Axis -1) to describe the extent of the equimomental ellipse lengthening or stretching.[15] Bleb-treated hMSCs demonstrated a significant reduction in alignment (52.26 % *versus* 88.19 %) and elongation (2.28 *versus* 7.75) as compared to untreated hMSCs after 7 days of culture on nanogratings (Figure 1C).

The hMSCs were then immunostained for the neuronal marker microtubule-associated protein 2 (MAP2), F-actin and nucleus using DAPI nucleic acid stain. Cells treated with Bleb or with the Rho kinase (ROCK) inhibitor Y27632 (100nM) showed fewer stress fibers than untreated controls on all substrates. Compared to control cells, Bleb also induced a smaller number of cellular processes while Y27632 did not affect the cell morphology. When hMSCs on nanogratings were cultured in either of the contractility inhibitors, MAP2 expression was abrogated (Figure 1D), indicating a role for actomyosin contractility in topography-induced differentiation. The results from RT-PCR verified the immunofluorescence staining observations (Figure 1E,F). The hMSCs that were cultured on nanogratings showed an upregulation of neuronal gene expression markers including MAP2, Nestin, Tyroxine Hydroxylase and Neurofilament-Light when compared to hMSCs cultured on unpatterned PDMS after 7 days. Both Bleb and Y27632 inhibited the upregulation of these neuronal markers by nanogratings in these hMSCs (Figure 1E). As nanotopography could also induce myogenic differentiation in hMSC,[10] we carried out similar experiments to investigate the effect of NM II inhibition on myogenic differentiation. The NM II inhibitors similarly inhibited the upregulation and expression of myogenic markers Pax3 and Myogenin (MYOG) in cells on the nanogratings (Figure 1F). These results collectively indicated the importance of actomyosin contractility in topography-induced hMSC differentiation.

Nanotopography Modulates Focal Adhesion (FA) Elongation and Focal Adhesion Kinase (FAK) Phosphorylation. We investigated the effect of topography on FA area and elongation by analyzing and quantifying paxillin expression in hMSCs cultured on gratings of different widths ranging

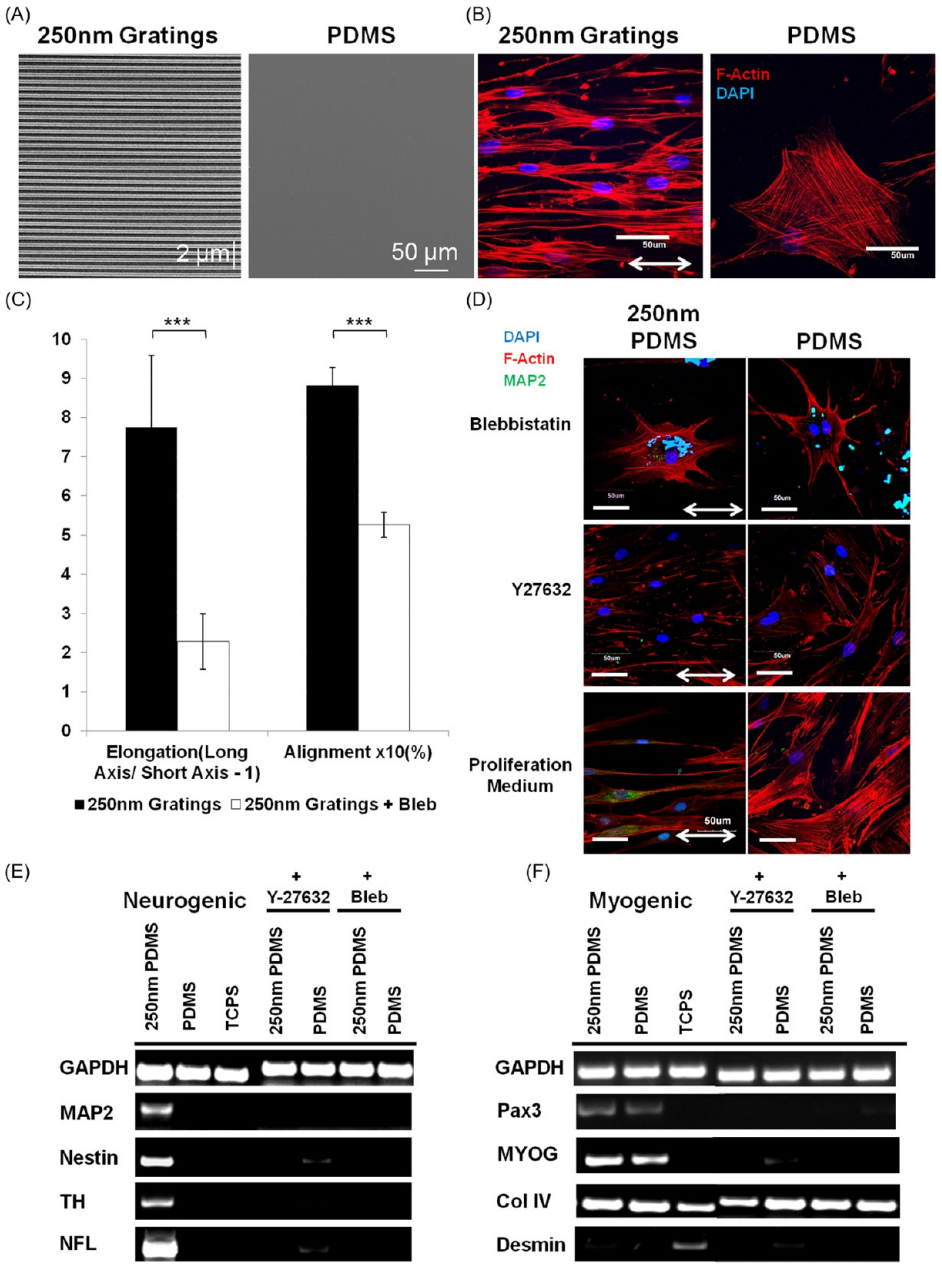

Figure 1. (A and B) Nanotopography characterization and cell morphology. (A) Scanning electron micrographs (SEM) of 250 nm gratings and unpatterned polydimethylsiloxane (PDMS) substrates and (B) fluorescently labeled human mesenchymal stem cells (hMSCs) on these substrates for F-actin (red) and DAPI (blue). (C−F) Nanotopography-induced alignment, elongation and differentiation of hMSC through actomyosin contractility. (C) Effect of Blebbistatin on the elongation and alignment of hMSCs on nanotopography (*$p < 0.001$, $n = 121$). (D) Immunofluorescence staining of hMSCs cultured with cytoskeleton contractility inhibitors on nanogratings for 7 days. A minimum of 100 cells per sample were analyzed for 3 separate experiments (double ended arrows = grating axis, scale bars = 50 μm). (E) RT-PCR analysis of neuronal differentiation markers MAP2, nestin, tyroxine hydroxylase (TH) and neurofilament-light (NFL) in hMSCs cultured on nanogratings with inhibitors. (F) RT-PCR analysis of myogenic differentiation markers PAX3, myogenin (MYOG), collagen IV (Col IV) and desmin in a similar experiment. Tissue culture polystyrene (TCPS) cultured cells served as controls.**

from 250 nm to 10 μm (Figure S1). Compared to cells on unpatterned PDMS, cells on 1 and 10 μm gratings showed larger FA areas while cells on 250 nm gratings showed smaller FA areas (Figure 2A), indicating that the FA areas were affected by the grating widths. The histogram of hMSCs' FA areas on nano (250 nm) and micrometer-sized (10 μm) gratings showed that the FAs on the nanogratings were significantly smaller than the FAs on the 10 μm gratings (Figure 2C). Interestingly, the FA elongation was also dependent on grating widths. FAs on gratings with sizes smaller than 1 μm were significantly more elongated than FAs on micrometer size gratings and unpatterned PDMS (Figure 2B,D). These results were consistent with our previous observations that cells were able to sense the differences between micrometer and nanosized

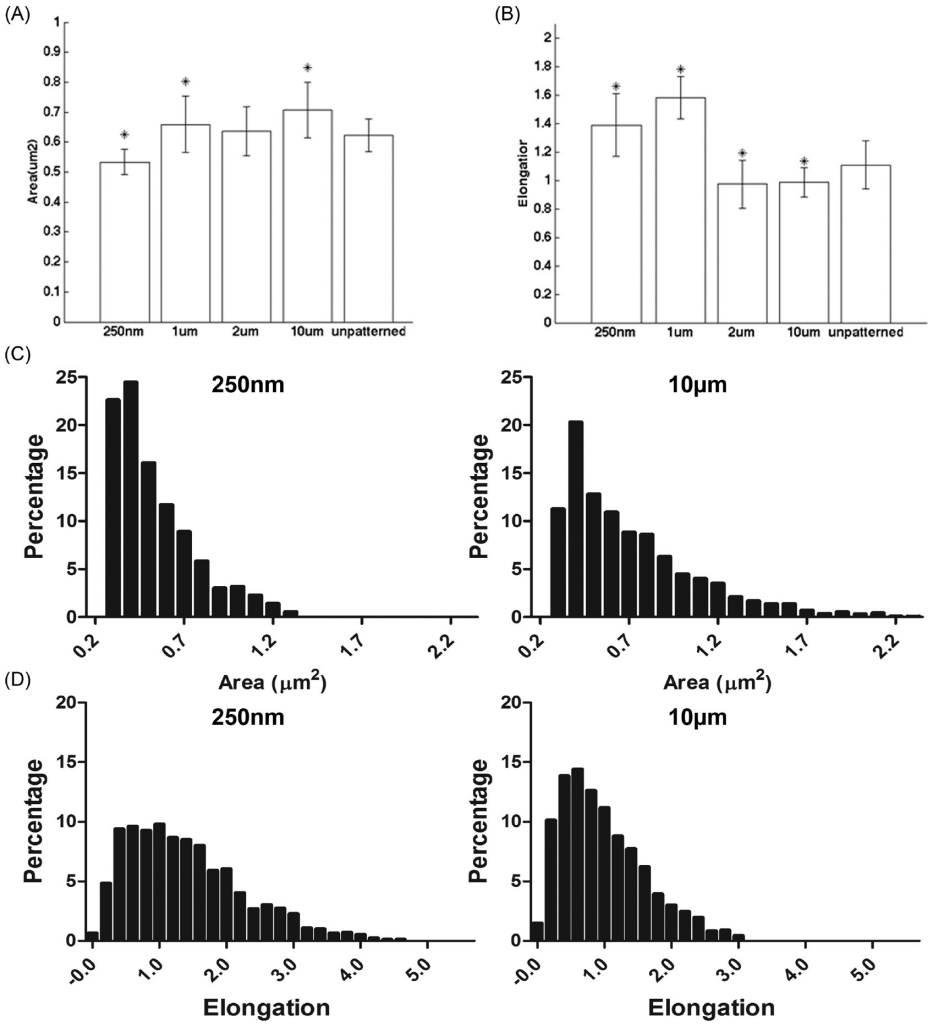

Figure 2. Nanotopography modulates Focal adhesion (FA) size and elongation. Quantification of the (A) area and (B) elongation of FA in hMSCs on different grating widths (*$p < 0.05$ *vs* unpatterned PDMS, $n = 3$). Histogram showing the frequency distribution of (C) FAs *vs* area and (D) FAs *vs* FA elongation on 250 nm nanogratings and 10 μm microgratings. See also Figure S1.

features,[9] showing that nanogratings can significantly alter the area and elongation of hMSCs' mature FAs compared to unpatterned substrates. More importantly, these data suggest the exciting possibility that extracellular nanotopographical cues may be transduced by hMSCs through the spatial arrangement of the FA.

Influence of Extracellular Matrix (ECM) on Topography-Induced Neuronal Differentiation. Since ECM could activate different integrin subsets, we were interested to investigate the effect of different ECM on the topography-induced neuronal differentiation and its relation to FAK activity. HMSCs were cultured on nanogratings and unpatterned PDMS substrates coated with fibronectin (FN), vitronectin (VN), laminin (LN), collagen I (Col I) or poly-L-Lysine (PLL) in serum-free medium. PLL-coated substrates allowed cell adhesion without integrin engagement. With the exception of PLL-coated substrates, the immunofluorescently-labeled hMSCs were observed to align and elongate according to the grating axis on all other ECM coated nanogratings substrates at day 7 (Figure 3A). Notably, cells did not favor adhering on PLL-coated substrates, resulting in the rounding of these cells.

An early (day 2) gene expression analysis using RT-PCR showed that LN coating alone upregulated MAP2 gene expression, while topography was able to induce MAP2 gene expression in substrates coated with FN, COL I or LN after 7 days. We also observed that MAP2 expression was strongly upregulated in hMSCs on LN-coated nanograting substrates, suggesting that there is a synergistic effect from LN coating and topographical cues (Figure 3B). Cells were also immunostained for MAP2 on different ECM-coated substrates (Figure S2), which showed a good agreement with the gene expression data after 7 days. As different ECM coatings were observed to regulate MAP2 gene and protein expression with or without topographical cues, we hypothesize that topography-induced neuronal gene expression on the various ECM-coated substrates were regulated by FAK activity. Western blot analysis of the hMSCs after 3 days of culture showed varying levels of phosphorylated tyrosine-397 FAK

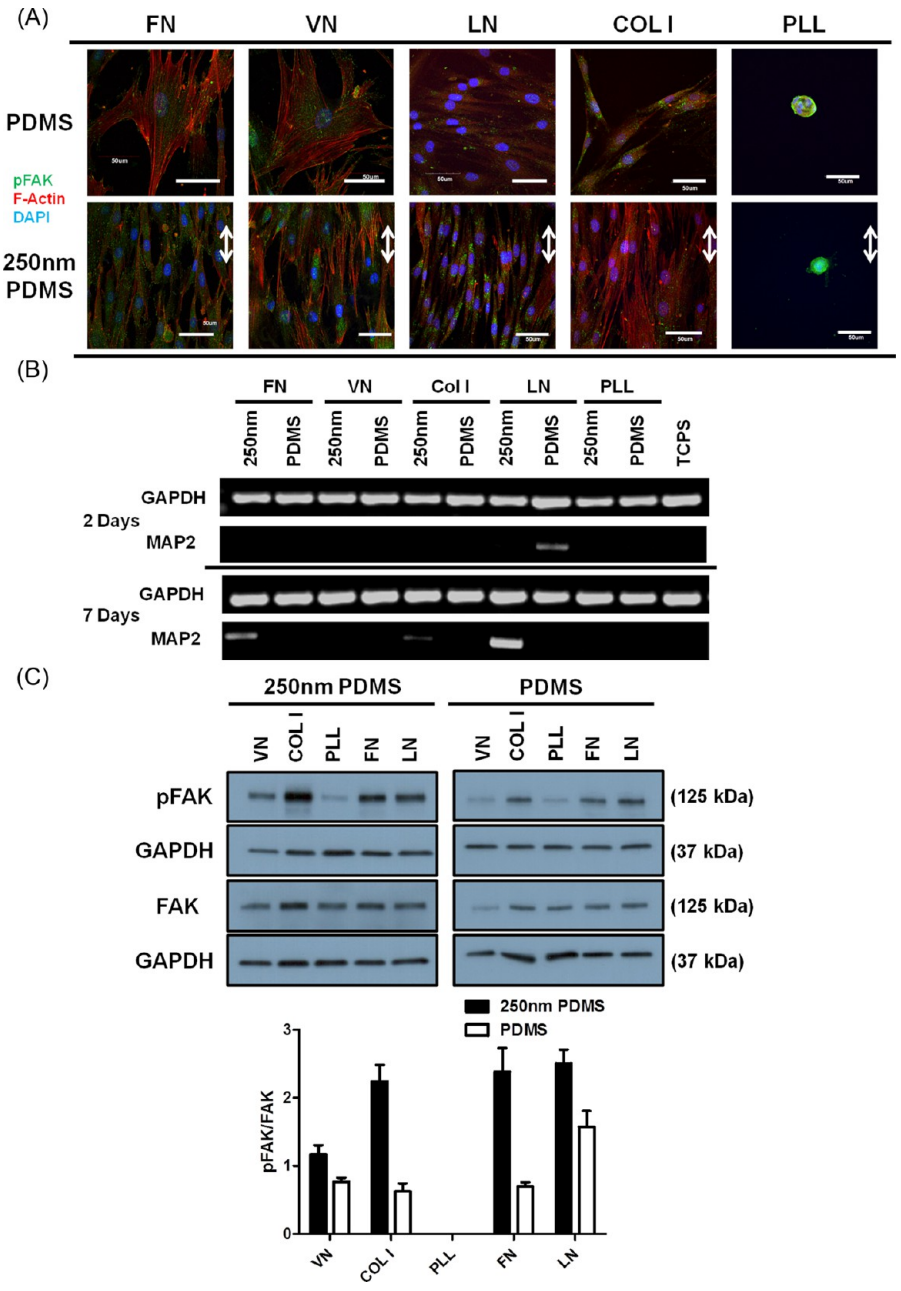

Figure 3. Influence of extracellular matrix on neuronal differentiation. (A) Immunofluorescence staining of hMSCs after 7 day culture on unpatterned (top row) and nanopatterned (bottom row) substrates coated with fibronectin (FN), vitronectin (VN), laminin (LN), collagen I (Col I) and poly-L-lysine (PLL) (scale bar = 50 μm, double ended arrows = grating axis). (B) RT-PCR analysis of MAP2 on nanopatterned and unpatterned substrates coated with different ECM after 2 and 7 days of culture. TCPS cultured cells served as controls. (C) Representative Western blot analysis for phosphorylated focal adhesion kinase (pFAK) and FAK expression levels in hMSCs on these substrates after 3 days of culture shown with the corresponding mean densitometric analysis (n = 3).

(pFAK) on these different substrates (Figure 3C). On average, cells on nanogratings showed higher levels of the pFAK/FAK ratio than cells on unpatterned substrates. Comparing among the nanogratings, the relative pFAK/FAK ratio showed LN > FN > COL I > VN≫PLL, indicating high levels of pFAK activity on LN, FN and COL I ECM. The pFAK/FAK ratios suggest a correlation between MAP2 neuronal gene expression (day 7) and the levels of FAK phosphorylation (day 3). FN coated substrates were used for subsequent experiments to reduce ECM-induced bias on hMSC differentiation.[16] Western blot densitometry analysis of hMSCs on nanogratings showed higher pFAK/FAK ratios (approximately 2-fold) than cells on unpatterned controls (Figure 4A). The results suggest that topography-induced hMSC differentiation undergoes a direct force-dependent mechanism through FAK to transduce topographical signals to the nucleus.

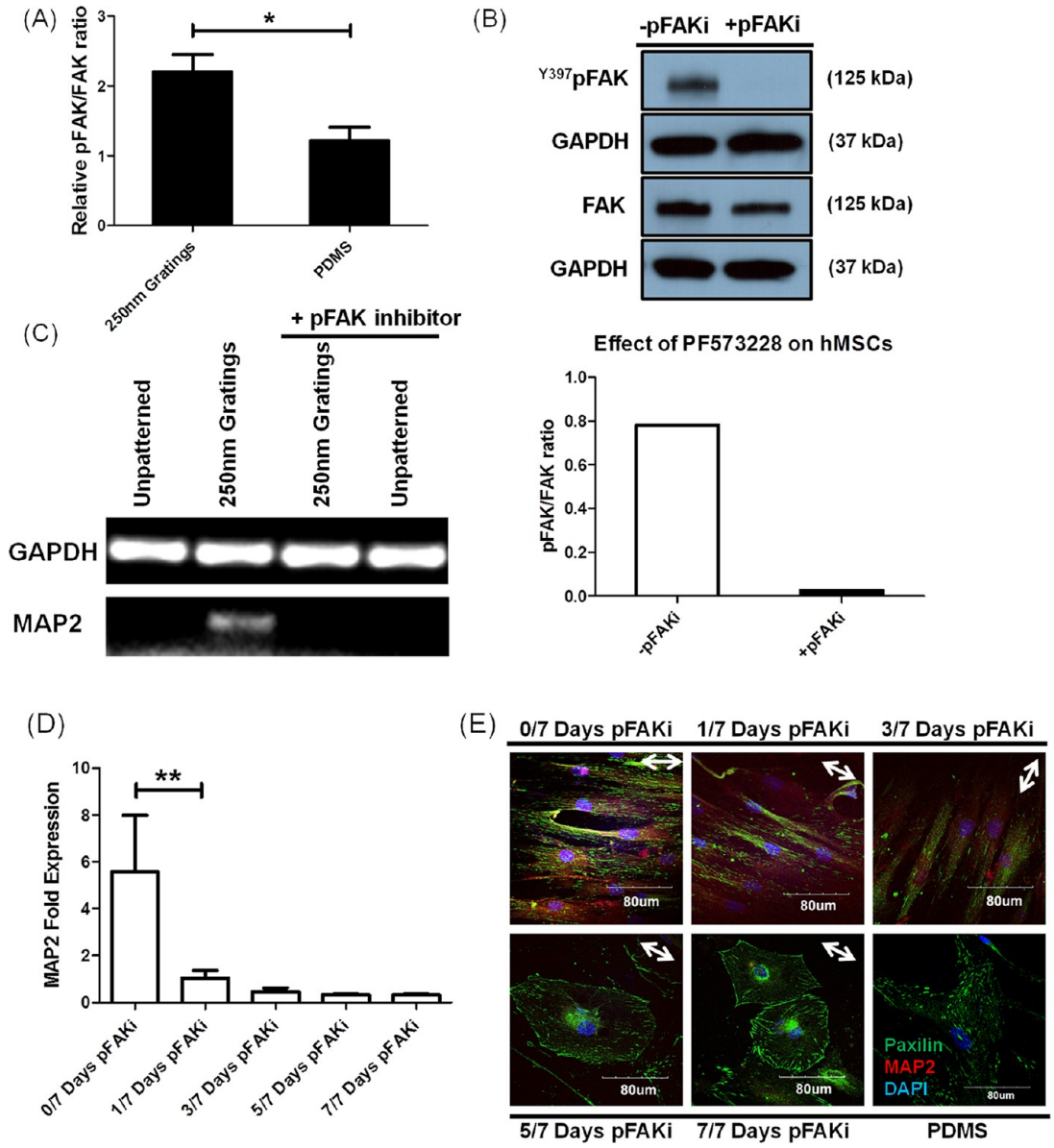

Figure 4. Y397-FAK inhibitor (pFAKi) PF573228 inhibits topography-induced differentiation (A) Comparative densitometric analysis of pFAK protein levels in hMSCs on nanogratings and unpatterned PDMS after 7 days of culture (*$p < 0.05$ *vs* unpatterned PDMS, $n = 3$). (B) Effect of PF573228 on pFAK protein levels of hMSCs on PDMS substrates after 7 days of culture. (C) RT-PCR analysis of the MAP2 in hMSCs cultured on 250 nm gratings and unpatterned PDMS substrates after 7 days with the addition of pFAKi. (D) Quantitative PCR analysis of MAP2 on nanogratings for different time periods of pFAKi incubation ($p < 0.01$ 0/7 days pFAKi *vs* all other groups, $n = 4$). (E) hMSCs immunofluorescence images for different pFAKi incubation periods after 7 days (double ended arrows = grating axis, scale bars = 80 μm).**

Y397-FAK Inhibitor (pFAKi) PF573228 Inhibits Topography-Induced Differentiation. To investigate the role of FAK phosphorylation and activation in topography-induced hMSC differentiation, a small molecule inhibitor of Y397-FAK autophosphorylation,[17] PF573228 (100 nM) was used with minimal cytotoxicity to cells (Figure S3). Western blot analysis of the hMSCs with 3 days of pFAKi treatment showed 5-fold lesser FAK phosphorylation than the untreated cells. The pFAKi-treated cells maintained native FAK expression (Figure 4B) with no visually apparent changes to their morphology when fully spread. We then cultured hMSCs on nanogratings with the addition of pFAKi for 7 days. When pFAK was inhibited using pFAKi during the 7-day culture, MAP2 upregulation was abrogated in the hMSCs (Figure 4C). The experiment indicated the importance of FAK phosphorylation in topography-induced upregulation of MAP2 expression.

By varying periods of pFAKi incubation, we observed that MAP2 expression was a function of pFAKi incubation time (Figure 4D). The MAP2 expression significantly decreased in all periods of pFAKi incubation but most significantly during the first 24 h. When the hMSCs were analyzed for phenotypic and FA changes during these periods, the typical elongated and aligned cell morphology on nanogratings

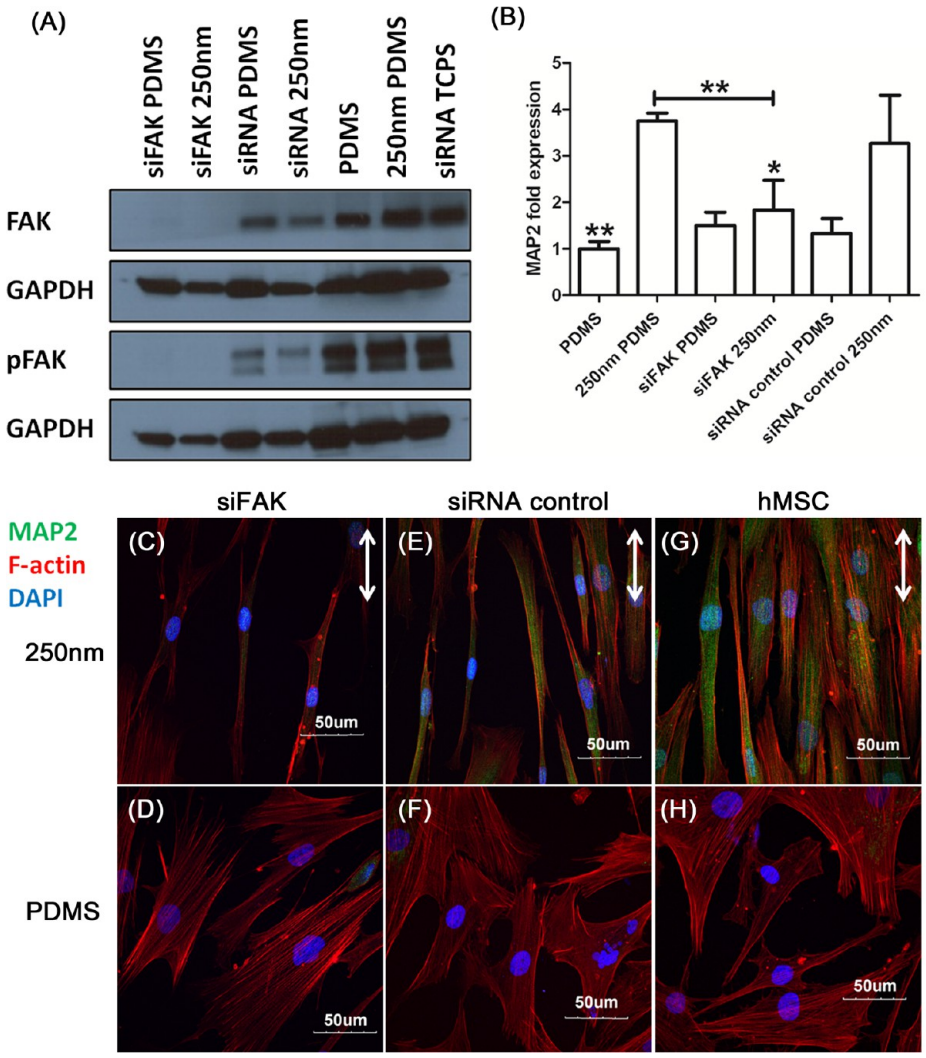

Figure 5. FAK siRNA inhibits topography-induced hMSC neuronal differentiation. (A) Western blot analysis for FAK and pFAK expression in these cells cultured on the various substrates after 7 days (B) Quantitative PCR analysis of MAP2 in siFAK hMSCs on all substrates. Immunofluorescence images of (C and D) FAK siRNA (siFAK), (E and F) antisense siRNA control hMSCs, and (G and H) untransfected hMSCs on the various substrates labeled for MAP2 (double ended arrows = grating axis, scale bars = 50 μm). Data are the mean $\pm$ SEM of three independent experiments ($p < 0.01$; *$p < 0.05$ *vs* siRNA control 250 nm).**

transitioned to a rounded and enlarged morphology with increasing periods of pFAKi incubation (Figure 4E). After longer periods of pFAKi incubation, hMSCs also showed increased paxillin expression that was concentrated in the cell periphery. Microspikes typical of nonpolar cell spreading were also observed in hMSCs incubated with pFAKi beyond 5 days. Although MAP2 expression appears to correlate with cell shape, the reduced MAP2 expression in the elongated hMSCs after 3 days of pFAKi treatment suggests that hMSC's MAP2 expression was not dependent on cell shape, but rather primarily regulated by the early activation of FAK in response to the topography.

Effect of FAK Inhibition Using FAK siRNA on hMSCs Morphology, FAK Phosphorylation, and Neuronal Differentiation. We further investigated the role of FAK by transfecting hMSCs with FAK siRNA (siFAK) using Lipofectamine RNAiMAX transfection reagent. An optimized concentration of 25nM FAK siRNA and the scrambled controls was used (Figure S4A-B). The siFAK-transfected hMSCs showed decreased pFAK intensity when visualized using immunofluorescence staining (Figure S4C). The Western blot analysis after 7 days showed decreased expression of pFAK and FAK in siFAK-transfected hMSCs on both nanogratings and unpatterned substrates (Figure 5A). Furthermore, the siFAK-transfected hMSCs on nanogratings also showed reduced MAP2 gene upregulation (Figure 5B). Similarly, neuronal marker was not detected in the immunostaining for MAP2 in the siFAK-transfected hMSCs, although they remained aligned to the nanogratings (Figure 5C–H). The reduction in neuronal marker upregulation reiterated the role of FAK in topography-induced hMSC differentiation.

`SuperFAK' hMSC Enhanced Topography-Induced Neuronal Differentiation. To investigate the effect of FAK hyperactivity on topography-induced neuronal differentiation,

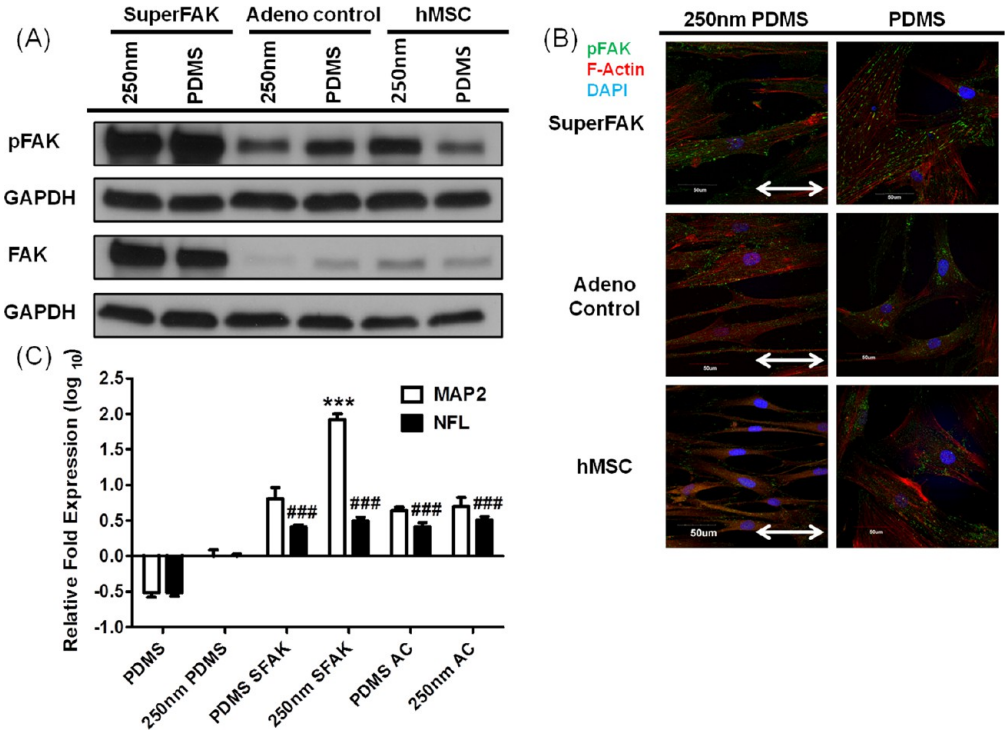

Figure 6. SuperFAK hMSCs on nanotopography showed enhanced neuronal gene expression (A) Western blot analysis of pFAK and FAK of SuperFAK-infected hMSCs (SuperFAK), adenocontrol (AC) and uninfected hMSCs on all substrates 7 days post adenoviral-infection. (B) Immunofluorescence images of SuperFAK hMSCs after seven days. (Double ended arrow = grating axis, scale bars =50 μm) (C) Quantitative PCR analysis of MAP2 and NFL in SuperFAK hMSCs (SFAK), adenocontrol (AC) and uninfected hMSCs cultured on different substrates after 7 days (*$p < 0.001$, *vs* 250 nm AC. ###$p < 0.001$ NFL *vs* 250 nm PDMS, $n = 3$).**

hMSCs were infected with the SuperFAK adenoviral construct to produce constitutively active FAK hMSCs (`SuperFAK') *in vitro* (Figure S5). `SuperFAK' is an activated mutant of FAK in which the catalytic activity is independent of cell adhesion but the tyrosine phosphorylation of downstream targets is adhesion dependent.[18] These SuperFAK hMSCs were then cultured on nanogratings to evaluate the effect of nanotopographical cues on enhanced FAK signaling. The increased levels of pFAK in these SuperFAK hMSCs was observed even in the absence of topographical cues (Figure 6A). SuperFAK cells, which were probed for F-actin and pFAK F-actin by immunofluorescence, showed a higher number and intensity of stress fibers and pFAK positive adhesions (Figure 6B) after 7 days of culture than the adenocontrol infected cells (AC). On nanogratings, SuperFAK hMSCs aligned to the grating axis, but were less elongated compared to the AC and uninfected hMSCs (250 nm PDMS). The quantitative PCR analysis showed that SuperFAK hMSCs showed a significant upregulation of MAP2 and NFL, even in the absence of topographical cues (Figure 6C), and a smaller, nonspecific upregulation of MAP2 and NFL in AC infected hMSCs. These SuperFAK hMSCs were also positive for MAP2 using immunofluorescence staining (Figure S5C). Our data showed that nanotopography and FAK hyperphosphorylation could synergistically upregulate the MAP2 expression, exhibiting levels approximately 83-fold and 13-fold higher than those observed in hMSCs on nanogratings and SuperFAK hMSCs on PDMS substrates, respectively.

DISCUSSION

Nanotopography can provide important physical cues to control stem cell differentiation (reviewed in Teo *et al.*[19]); however, the exact mechanism of topography-induced cellular behavior remains unclear. The effect of topography is most evident when hMSCs are cultured on nanogratings, where they align and elongate themselves to the grating axis. Interestingly, the use of nanogratings was able to bias the hMSCs to differentiate toward the neuronal and myogenic lineages without the use of any biochemical factors.[9,10] We hypothesize that topography-induced hMSC differentiation occurs through mechanotransduction, where signals from the underlying topography are transduced through the focal adhesions (FAs) to the actin-CSK before shaping the nucleus to influence cellular gene expression. Our results indicated that actin-CSK contractility was important in determining hMSCs' reaction to topography. Bleb significantly reduced the alignment and elongation of the hMSCs on nanogratings. More importantly, the inhibition of NM II activity using either Bleb or Y27632 abrogated the upregulation of neuronal maker MAP2. Gene expression

analysis for both neuronal and myogenic markers showed that contractility inhibition overruled the topographical control of characteristic lineage differentiation. The contractility-impaired hMSCs were unable to transduce topographical cues, therefore displayed uncharacteristic cell morphology and lineage bias on topographical substrates. These observations were consistent with an earlier study using substrates without topographical cues but of different stiffness.[7] In that study, contractility inhibited hMSCs were unable to sense different stiffness cues from the underlying substrates. A more significant change in cell morphology on nanotopography was observed in our study. This was possibly due to the increased intracellular contractile force on our topographical substrates, where the effect of the blocking of NM II appeared to be stronger. The downregulated neuronal and myogenic markers were indicative of the importance of CSK NM II feedback for the mechanotranduction process in topography-induced cell shape modulation and stem cell differentiation.

The transduction of topographical information into morphological changes and lineage differentiation requires a sensing mechanism that is postulated to require the contractility of the CSK against the ECM, and these CSK-dependent generated signals regulate the FA formation and maturation.[20] Our earlier study showed grating width to be a determinant of MAP2 gene expression, where nanosized gratings gave the highest upregulation of neuronal markers.[9] When we characterized the FA on different grating widths, both FA area and elongation were modulated by nanotopography. Interestingly, the FA elongation but not the FA area was more indicative of the topographical response. The increase of FA elongation when the grating width decreased from 2 to 1 μm showed that hMSCs have an intricate sensing mechanism that differentiates between micrometer and nanosized topographies. We believe that topography compartmentalized FA components in a regulated spatial arrangement as a signal for cell differentiation. As the observed adhesion size distribution lies within the range for stable mature FAs, the hMSCs on these different grating widths were likely to be in a steady state. These hMSCs on different grating widths would exert a net force similar to each other dependent on the substrate bulk rigidity (PDMS, E = 1.5 MPa). However, different grating widths can restrict FA elongation causing hMSCs to adopt different contractility-force profile distributions. The CSK contractility of an elongated cell will be unlike that of a spread-out cell due to differences in the CSK-FA pulling angle.[21] This could be a possible mechanism of different force transmission through the CSK contractility. Thus, nanogratings could regulate the necessary FA spatial organization to induce the differentiation of hMSCs, in particular through the elongation of FA components.

Different ECM composition can direct stem cell differentiation *via* distinct integrin pathways.[22] Our mechanistic study eliminates the need for differentiation factors which makes the study less convoluted. We hypothesize that these ECM coatings affect hMSC differentiation through the initial regulation of FAK phosphorylation. The increase in pFAK across all ECM *via* topography, except PLL, was indicative of FAK as an important mediator of topographical signals. Day 2 laminin-induced MAP2 expression possibly went through specific interactions between binding sites and cell surface receptors independent of topographical control of cell differentiation.[23] The effects of topography were more evident after 7 days. The highest MAP2 upregulation observed on LN coated nanopatterned substrates at day 7 suggested a synergy between LN and topographical control of differentiation. Topographical-induced MAP2 upregulation on FN, Col I and LN coated nanopatterned substrates were interestingly correlated with increased pFAK/FAK levels, recapitulating aspects of FAK signaling in transducing topographical cues into post-translational responses. Topographically-induced hMSC neuronal differentiation was thus dependent on actomyosin contractility and pFAK but not dependent on direct ECM-induced pathways.

The FAs bridge the CSK network to the ECM and thus could be important sensors of topography.[24] The hMSCs on nanotopography showed lower expression of integrin subunits α_2, α_V, α_6, β_2, β_3 and β_4 than cells on unpatterned substrates,[11] suggesting that the topographical signals can be transduced *via* the differential integrins to the FAs signaling components. Focal adhesion kinase (FAK) is one such signaling molecules that upon integrin activation, autophosphorylates at the Y397 site before binding and phosphorylating Src-family tyrosine kinases. Interestingly, the Src-family kinases are highly enriched in nervous systems and are involved in axon guidance signaling.[25] In our study, we showed that FAK regulates topographical control of hMSC neuronal differentiation mediated *via* the integrins and CSK contractility.

The increased Y397-FAK phosphorylation in the hMSCs on nanotopography indicated that topography is able to increase FAK activation. The specific inhibition of pFAK abrogated the upregulation of neuronal markers in hMSCs cultured on topography, indicating the importance of FAK in topography sensing and the induced differentiation. The results showed that FAK is an upstream mechanosensor of the topography and possibly triggers a series of downstream pathways for the neuronal marker gene expression. A recent study of cellular motility indicating FAK's upstream recruitment to nascent adhesion sites, as opposed to talin, within the first 24 h of attachment[26] could lend support to FAK's role as an early mechano- or topography sensor.

To identify the time window of critical FAK activity for regulating topography-induced differentiation, pFAKi wash-out experiments were performed. From our data, FAK activity was critical for both topography sensing and induced differentiation during the first 24 h of hMSC adhesion. Taken together, these results were consistent with the time period of hMSC alignment to topography as well as FAK recruitment and activation. The blocking of FAK phosphorylation would indirectly impede the feedback signals between integrin-FAK-CSK, which were crucial for the topography sensing and induced differentiation. Since increasing periods of pFAK inhibition were able to reduce the MAP2 expression, FAK-regulated transcriptional control is implicated.

The transitions from aligned and elongated hMSCs into the rounded and spread out morphology upon pFAK inhibition were consistent with the earlier observations in FAK$^{-/-}$ cells.[27] The rounded cell morphology observations corresponded to an early stage of nonpolarized cell spreading,[28,29] which indicated that topographical cue sensing requires FAK phosphorylation. The pFAKi causes FA turnover failure, impairing migratory response of hMSCs on topographical cues, leading to stronger cell-substrate adhesions and the observed nonpolarized cell state. The observations of elongated cell morphology even after 3 days of pFAKi incubation, yet a corresponding low MAP2 gene and protein expression, suggest that FAK had a more direct effect on MAP2 expression as compared to cell shape. Using another method to knockdown the FAK expression, the reduced MAP2 gene expression in the siFAK hMSCs confirmed the role of FAK in topography induced hMSC differentiation. Our findings showed early FAK activity to be critical in topography sensing and subsequently gene regulation in stem cells.

SuperFAK hMSCs provided an elegant approach to investigate adhesion dependent hyperphosphorylation of FAK on nanotopography. When the hyperactive SuperFAK hMSCs were used, the signaling activity (*via* tyrosine phosphorylation) of FAK upon adhesion to culture surfaces was greatly enhanced. The SuperFAK cells also retained the ability to recruit downstream Src kinases. In the absence of topographical cues, SuperFAK hMSCs on unpatterned substrates showed higher MAP2 upregulation than the uninfected hMSCs on nanogratings, revealing the significance of FAK phosphorylation in hMSC differentiation. Although we observed nonspecific upregulation in the adenocontrol infected cells, SuperFAK hMSCs cultured on nanogratings showed the highest upregulation of MAP2 gene expression, indicating the amplification of pFAK signaling (and thus MAP2 expression) through topography. FAK hyperactivity primed SuperFAK hMSCs hyperactivates the downstream signaling pathways in response to topographical stimulation, enhancing the differentiation. However, late marker NFL gene expression was not as upregulated possibly due to the inadequate maturation of these neuronal differentiated hMSCs, since specific neuronal factors were absent throughout the culture period.[30] We repeatedly observed a correlation between MAP2 gene expression and hMSCs pFAK/FAK levels in all ECM, pFAKi and SuperFAK experiments. The findings collectively suggest that the phosphorylation of FAK possibly acts as a signal transducer between integrins and the CSK to relay the topographical cues to the nucleus *via* the intracellular contractility. Mechanistically, topographical cues could stimulate CSK tension dependent YAP/TAZ transcriptional regulators through FAK to dictate cell lineage.[31]

CONCLUSION

In this study, we identified and examined the crucial role of focal adhesions in the nanotopography-induced stem cell differentiation. We showed that the dimensions of the underlying nanotopography can modulate the focal adhesion characteristics within the human stem cell. In particular, the FA size and elongation in the hMSCs were significantly different on the nanogratings compared to the microgratings, suggesting a size-dependence in the FA regulation. It is likely that adherent stem cells require inter-FA component crosstalk to sense the ECM topography and regulate various cellular functions. Our findings showed FAK to be one of the important early mechanosensors of ECM topography. The increase in FAK phosphorylation was observed on substrates with different ECM compositions. We also observed a correlation between FAK phosphorylation and neuronal gene marker upregulation, demonstrating that hMSCs neuronal lineage differentiation was primarily dependent on the spatial and temporal regulation of FAK phopshorylation. Further detailed investigations of other cellular components involved in the mechanotransduction process can aid our understanding of how stem cells communicate the physical signals from nanotopographical substrates.

MATERIALS AND METHODS

Nanogratings Fabrication and Surface Preparation. The nanogratings was initially produced using nanoimprint lithography as previously described.[3] The polydimethylsiloxane (PDMS) nanogratings were fabricated using soft lithography on the nanoimprinted poly(methyl methacrylate) (PMMA) coated silicon master mold. The gratings on the nanoimprinted PMMA master molds were 250 nm in depth, 250 nm in width and 500 nm pitch (center to center) unless otherwise stated. The replicated patterned PDMS substrates were air plasma-treated (Femto Science, CUTE-B, Korea) at 80% power for 1 min and coated with 2 μg/cm^2 of bovine fibronectin (Biological Industries, Bio-REV, Singapore) to increase cell adhesion on the hydrophobic

PDMS. To study the correlation of focal adhesion arrangement, gratings of 1 μm and 10 μm widths, with respective 2 and 20 μm pitches, were also fabricated similarly. All gratings had the same depth of 250 nm. All substrates were coated with fibronectin unless otherwise stated.

Cell Culture. HMSCs (Poietics hMSC, Lonza Singapore) were grown and maintained in MSCGM medium (Lonza) at 37 °C in a 5% CO_2 incubator. hMSCs from passages 4−6 were seeded on substrates at 5×10^3 cell/cm^2. Analyses of differentiation were performed after a 7-days culture period unless otherwise specified.

Immunofluorescence Staining. At the end of the 7-days culture, immunofluorescence staining of focal adhesion kinase (FAK), phosphorylated FAK (pFAK), paxillin or microtubule-associated protein 2 (MAP2) was performed on the cells according to a standard immunofluorescence staining procedure. The cells were first fixed in 4% paraformaldehyde (PFA, Sigma-Aldrich, Singapore) for 15 min, then permeabilized with 0.1% Triton-X100 (Bio-Rad, Singapore) for 15 min followed by blocking in 1% bovine serum albumin (BSA, vCell Science, Singapore) for an hour. Primary and secondary antibody incubation was carried out at 4 °C overnight, while nuclei and F-actin were counterstained, respectively, with 4′,6-diamidino-2-phenylindole (DAPI, Sigma-Aldrich, 1:5000 (1 ng/μL)) and F-actin phalloidin (1:500 (6.6 μM)) for 20 min. The F-actin phalloidin used was either conjugated with Oregon Green 488 or Alexa Fluoro 546 (Molecular Probes, Life Technologies, Singapore). Primary antibodies were diluted in 1% goat serum in phosphate buffered saline (PBS) while secondary antibodies were diluted in PBS. Primary antibodies used included rabbit anti-phosphorylated Y397 FAK antibodies (pFAK, Abcam, Cambridge, MA, USA, 5 μg/mL), mouse anti-MAP2 primary antibodies (Abcam, 4.4 μg/mL) and rabbit antipaxillin primary antibodies (Abcam, 1:250). The staining for MAP2 indicated neuronal differentiation since it is a neuronal marker found predominantly in mature neurons.[32] Secondary antibodies Alexa-Fluor546 goat antimouse secondary antibodies and Alexa-Fluor488 goat antirabbit antibody (Molecular Probes, Life Technologies, Singapore) were used at 1:1000 dilutions. The samples were then visualized with Olympus FluoView FV1000 (Olympus, Japan) laser scanning confocal microscope using a 60×/1.00 water objective, with 488 nm Argon or 543 nm HeNe laser as the excitation source. Images were then viewed and converted to appropriate formats using the attached FV10-ASW v1.7 software.

mRNA Gene Expression Profile. Total RNA was isolated from cells cultured on the respective substrates at appropriate time points using the Trizol Reagent (Invitrogen, Life Technologies, Singapore). The isolation of RNA was done according to the protocol recommended by Invitrogen. The quantity and quality of RNA was measured and only the samples with the 260 nm to 280 nm ratio greater than 1.85 were used for downstream applications. After isolation of RNA, neuronal markers such as MAP2, nestin, tyroxine hydroxylase (TH) and neurofilament (NFL) and myogenic markers such as Pax3, collagen IV (Col IV), Desmin and Myogenin (MYOG) primers were used in reverse transcription polymerase chain reaction (RT-PCR) while glyceraldehyde 3-phosphate dehydrogenase (GAPDH) served as an endogenous control. Primers used are listed in Table S1 (1st BASE, Singapore). Synthesis and amplification of DNA were performed using the Qiagen one-step RT-PCR kit in accordance with the manufacturers' protocol (Qiagen, Singapore). The PCR was carried out for 37 cycles with an annealing temperature of 59 °C for the neuronal markers, while the annealing temperature used for the myogenic markers was 51 °C. PCR products were then resolved on 1.2% agarose gel in TAE buffer.

Real-Time PCR. The quantitative gene expression of MAP2 and NFL were analyzed by real-time PCR using GAPDH as the endogenous control. Reverse transcription was performed with a Sensiscript RT kit (Qiagen, Singapore) with an Oligo(dT)$_{12-18}$ Primer (Invitrogen). PCR was performed using TaqMan Universal PCR Master Mix (Applied Biosystems, Life Technologies, Singapore) with human MAP2 and human NFL Taqman Gene Expression Assays primer and probes (Applied Biosystems) and human GAPDH (Applied Biosystems) as endogenous control. The PCR cycling consisted of 40 cycles of amplification of the template DNA with a primer annealing at 60 °C (15 s). The real-time PCR was performed on an Applied Bioscience Thermocycler (7500 Fast). The RNA levels were normalized to the GAPDH mRNA level. Data presented were normalized to RNA level expressed in the hMSCs control.

Western Blot of pFAK and FAK Protein Expression. Total proteins from the hMSCs cultured on the respective substrates at appropriate time points were isolated using the RIPA buffer (Thermo Scientific, Fischer Scientific, Singapore). Phenylmethanesulfonyl fluoride and sodium orthovanadate were added to the RIPA buffer at a concentration of 1 mM to inhibit serine, cysteine proteases and tyrosine phosphatases, respectively. The cells were washed twice with ice-cold PBS before the cocktail was added to the well plates and incubated for 5 min. Samples were then maintained under constant agitation for 30 min at 4 °C followed by centrifugation at 12000*g* at 4 °C for 20 min. The supernatant containing the isolated protein is then concentrated using Vivaspin 500 Centrifugal Concentrator (Sartorius Stedim Biotech, Singapore). The quantification of protein was done using a micro BCA assay (Thermo Scientific). Equal amount of protein samples were mixed with Laemmli 2× buffer (Sigma) in a ratio of 1:1 and denatured by heating at 95 °C for 5 min. The mixture was then loaded into the gel and electrophoresis was carried out at 200 V for 1 h in 1× Tris-glycine buffer (1st BASE, Singapore). A sodium dodecyl sulfate−polyacrylamide gel electrophoresis (SDS-PAGE) was performed using a 7.5% polyacrylamide gel. The separated protein in the gel was then transferred to a polyvinylidene fluoride membrane. The procedure was done in transfer buffer (10% 1× Tris-glycine-SDS (1st Base), 20% methanol, 30% deionized (DI) water) at 100 V for 1 h at 4 °C. The membrane was blocked using 5% BSA and 1% glycine dissolved in Tris buffer saline with Tween20 (TBST) buffer to prevent nonspecific background binding for 1 h with agitation before being washed twice with TBST with 5 min incubation per wash. Primary antibody incubation was done overnight at 4 °C while secondary antibody incubation was carried out for 1 h with agitation. The primary antibodies used were mouse anti-GAPDH antibody (1 μg/mL, Santa Cruz), rabbit anti-FAK antibody (Cell Signaling Technology, Research Biolabs, Singapore) and rabbit anti-pFAK primary antibody (0.5 μg/mL, Abcam). Horseradish peroxidase (HRP) conjugated anti-mouse and anti-rabbit secondary antibodies (Bio-Rad) were used at 1:1000 and 1:10000 dilution, respectively. The membranes were then washed 3 times (10 min incubation per wash) using TBST between the antibody-incubations. Chemifluorescence signals were generated using ECL Plus Western Blotting Detection Reagents (GE Healthcare, SciMed (Asia), Singapore) and imaged using X-ray sensitive films. Densitometry was performed using the BioRad Quantity One program for quantitative analysis.

Focal Adhesion (FA) Quantification, Alignment, and Elongation Characterization. To quantify FA, the hMSCs on the various grating width substrates were immunofluorescently stained for FA protein component paxillin. Using image processing software ImageJ, Fiji (http://fiji.sc), the color depth of each image was first converted to 8-bit before adjusting for background corrections. As a preprocessing step to improve the identification of focal adhesions, the local contrast of each image was then enhanced using the CLAHE algorithm.[33] Subsequently, the image was converted to binary mode with the focal adhesions showing as black patches and the open operation was applied to remove speckle noise. The Analyze Particles tool in ImageJ was invoked to locate and count the focal adhesion patches. The size and circularity were set to be larger than 0.8 μm^2 and smaller than 1 μm^2, respectively. Manual curation was performed as the last step to eliminate malformed or non-well-defined patches. Four independent samples were examined for each grating size with nonpatterned substrates as controls. Fifteen separate regions of each sample were imaged using the Olympus Fluoview FV1000 (Olympus, Japan) laser scanning confocal microscope and converted to appropriate formats with FV10-ASW v1.7.

hMSC Cytoskeletal Contractility and Y397-FAK Inhibition. To inhibit the nonmuscle myosin II and Rho-associated protein kinase, Blebbistatin (50 μM) and Y-27632 (10 μM) were added into the hMSC cell suspension to be seeded onto the various substrates

(Tocris Bioscience, Sciencewerke, Singapore). The concentrations of Blebbistatin and Y-27632 (10 μM) used in hMSCs were previously documented in publications by other groups working with similar cell types.[34,35] As Blebbistatin is light sensitive, all cell cultures involving Blebbistatin were carried out in low light conditions throughout the experiment.[36] For Y397-FAK inhibition, PF573228 (100 nM, Tocris Bioscience) was used instead. Medium containing the individual inhibitors was changed on a daily basis. Elongation and alignment of the hMSC was analyzed using ImageJ, NIH image processing software (Bethesda, MD) on the fluorescent images with F-actin stained with Alexa Fluor 488 phalloidin (Life Technologies). The cell was considered to be aligned when the angle between the long axis of the cell and the grating was less than 15° while the elongation parameter describes the extent of the equimomental eclipse lengthening or stretching.[15] It was calculated as the ratio of Long Axis/Short Axis −1. The percentage of aligned cells in the measured population and elongation factor were measured. An average of 300 cells was counted for each sample, and $n = 3$ for each experimental group.

pFAKi Wash-Out Experiment. To determine the crucial period of FAK sensing of the topography, five parallel sets of experimental groups were carried out to investigate the temporal effect of pFAKi on MAP2 neuronal gene expression in hMSCs. For each group, hMSCs were cultured in pFAKi added medium for different time periods ranging from zero to seven days. pFAKi was added into the cell culture medium from the onset of cell seeding except for 0/7 days time point where no pFAKi was added. The pFAKi medium was replaced with basal hMSC proliferation medium (MSCGM) after the stipulated time period of FAK inhibition until the end of the experiment. All samples were used for RNA isolation or immunofluorescence staining after 7 days of culture from cell seeding.

Effect of ECM on FAK Phosphorylation and hMSC Neuronal Differentiation. To test the different ECM, nanopatterned and unpatterned PDMS substrates were all coated at 20 μg/mL with bovine fibronectin (Biological Industries, Bio-REV, Singapore), human recombinant vitronectin (Millipore, Research Biolabs, Singapore), rat type I collagen (BD Biosciences, Singapore), mouse laminin (Invitrogen) and poly-L-lysine (Sigma Aldrich). Substrates were coated in PBS for 1 h at 37 °C with the exception of collagen I and poly-L-lysine substrates which were carried out using 1 mM HCL and DI water, respectively. All substrates were rinsed three times with PBS after coating before cell seeding. Experiments investigating specific effects from ECM were carried out using serum free TheraPEAK Mesenchymal Stem Cell Chemically Defined Growth Medium (Lonza, Singapore). Samples were then used for immunofluorescence staining, Western blot or RNA isolation at appropriate time points.

FAK Inhibition by Small Interference RNA (siRNA) in Human Mesenchymal Stem Cells. The FAK gene expression in hMSCs was also inhibited using siRNA interference. Briefly, the cells for transfection were seeded on tissue culture 6 well plates and subsequently transfected with Silencer validated siRNAs targeting PTK2 (S11485, Ambion, Inc.) using Lipofectamine RNAiMAX transfection reagent (Invitrogen), according to the manufacturers' instructions. The siRNA and transfection reagent were reconstituted in OPTI MEM (Invitrogen) separately and then mixed together for 15 min to form transfection complexes giving a final siRNA concentration of 25 nM (Supporting Information Figure 4). The complexes were then dispensed onto the cells in six well plates and the medium was replaced with MSCGM after 24 h. Untransfected hMSCs and Ambion's validated Silencer negative control siRNA (Ambion, Inc.) transfected hMSCs were used as controls.

For siRNA studies on nanotopography, transfected hMSCs from the above-mentioned protocol were trypsinized and seeded onto the patterned or unpatterened PDMS. The FAK and pFAK levels were analyzed by Western blotting while neuronal marker expression was analyzed by real-time PCR and immunofluorescence staining after 7 days.

SuperFAK Adenovirus Amplification, MOI Determination, and hMSC Infection Efficiency. SuperFAK Adenovirus was produced by using the sequence information provided by Gabarra-Niecko *et al.*[18] The amplification of the virus was done using Human Embryonic Kidney (HEK) packaging cell line, 293T (ATCC). A 10 cm tissue culture dish was coated with Collagen solution (Cell-Matrix, 10 μg/mL, 1 mM HCl) for 30 min at 37 °C prior to plating cell. For the viral amplification process, HEK cells plated on the collagen coated dish were infected with 5 μL/mL of SuperFAK adenoviral stock solution for 4 days in DMEM (Invitrogen) supplemented with 10% FBS (Gibco, Life Technologies, Singapore) and 1% penicillin−streptomycin (Sigma). When all the cells were detached from the surface, the culture medium was collected and centrifuged to pellet the cell debris. Supernatants containing the virus were then divided into aliquots and stored at −80 °C. The supernatant went through a 3 cycle freeze thaw process to release the viral particles. To determine the multiplicity of infection (MOI), 293T cells were plated on 96 well plates and MOI was determined using a standard $TCID_{50}$ protocol. Similar experiments were done, using Adenovirus *Lac Z* (a gift from Dr. Keiko Kawaguchi, MBI Singapore) as a control. A MOI of 25 was chosen for infection. The hMSCs were exposed to viral supernatant for 24 h in serum free medium (Lonza) before being detached and seeded onto glass coverslips. The infection efficiency in hMSC was determined by immuno-fluorescence staining of pFAK, using adenocontrols and uninfected hMSCs as controls. Ten random images of each sample were taken using an epifluorescence microscope (Leica DM IRB) and counted for positively infected hMSCs as a percentage of uninfected hMSCs within the image ($n = 3$).

SuperFAK Protein Expression and Effect of Nanotopography on Super FAK hMSCs. hMSCs were plated at 20000 cells were cm^2 in a 6 well plate 24 h before infection. SuperFAK adenovirus and adeno *Lac Z* control at an MOI of 25 was used to infect the hMSCs for 24 h. The viral particles were then removed and the cells were washed with PBS thrice. The cells were then trypsinized and replated and grown for 3 days before being lysed as previously mentioned using ice-cold RIPA buffer and subsequently used for protein expression studies. For SuperFAK hMSCs seeding on patterned and unpatterened substrates, the cells were first infected using previously mentioned procedure before being trypsinized and seeded on the topographical substrates after 24 h. Cells were lysed for protein expression analysis 3 days after cells seeding while RNA isolation and immunofluorescence staining were performed on day 7 after cell seeding for neuronal differentiation analysis.

Statistical Analysis. All data were analyzed by one way analysis of variance (ANOVA) and Tuker's HSD test for posthoc multiple comparison analysis. Asterisks indicate *p-value <0.05, **p-value <0.01, and ***p-value <0.001. All values are mean ± standard deviation while error bars are standard deviations from independent experiments unless otherwise stated.

Conflict of Interest: The authors declare no competing financial interest.

Supporting Information Available: Figure S1 shows the scanning electron micrographs of all the patterned substrates used for focal adhesion quantification and the differences in paxillin formation of hMSCs dependent on the topography size. Figure S1 also shows the homogeneity of fibronectin coating on pattern and unpatterned substrates and their corresponding adsorbed fibronectin concentration on the substrate surface. Figure S2 shows hMSCs immunofluorescently labeled for MAP2 on different ECM coated substrates. Figure S3 shows cell viability assay of FAK inhibitor to determine the optimal concentration for hMSCs. Figure S4 shows the optimization of siFAK concentration in hMSCs using gene and protein expression. pFAK was also visualized by immunofluorescence staining. Figure S5 shows pFAK and FAK protein expression in hMSCs infected with different concentrations of adenovirus and immunofluorescence staining for pFAK in hMSCs infected with 25 MOI SuperFAK adenovirus. SuperFAK hMSCs were also immunofluorescently labeled for MAP2 on patterned and unpatterned substrates. Figure S6 shows the effect of contractility inhibitors on topography-induced hMSCs differentiation using an independent batch of hMSCs from a different donor. Shown in the figures are the immunofluorescent images and quantitative gene expression data for MAP2. Figure S7 shows a similar topography-induced differentiation and FAK involvement present in tissue culture polystyrene substrates using immunofluorescence

staining for MAP2. Table S1 summarizes the neurogenic and myogenic gene profiling primers used for RT-PCR. This material is available free of charge *via* the Internet at http://pubs.acs.org.

Acknowledgment. We thank M. Sheetz, A. Bershadsky, B. Ladoux, B. C. Low, and C. G Koh for scientific discussions, and K. Kawauchi for advice and gift of reagents for adenoviral viral infection. The work was supported by National Research Foundation Singapore under its Research Center of Excellence Programme and administrated by Mechanobiology Institute Singapore. B.K.K.T. is supported by NUS Research Scholarships funded by the MOE and S.T.W. is supported by the ASTAR Scientific Staff Development Award.

REFERENCES AND NOTES

1. da Silva Meirelles, L.; Chagastelles, P. C.; Nardi, N. B. Mesenchymal Stem Cells Reside in Virtually All Post-Natal Organs and Tissues. *J. Cell Sci.* **2006**, *119*, 2204–2213.
2. Dalby, M. J.; Gadegaard, N.; Tare, R.; Andar, A.; Riehle, M. O.; Herzyk, P.; Wilkinson, C. D. W.; Oreffo, R. O. C. The Control of Human Mesenchymal Cell Differentiation Using Nanoscale Symmetry and Disorder. *Nat. Mater.* **2007**, *6*, 997–1003.
3. Yim, E. K.; Reano, R. M.; Pang, S. W.; Yee, A. F.; Chen, C. S.; Leong, K. W. Nanopattern-Induced Changes in Morphology and Motility of Smooth Muscle Cells. *Biomaterials* **2005**, *26*, 5405–5413.
4. Teo, B. K.; Goh, S. H.; Kustandi, T. S.; Loh, W. W.; Low, H. Y.; Yim, E. K. The Effect of Micro and Nanotopography on Endocytosis in Drug and Gene Delivery Systems. *Biomaterials* **2011**, *32*, 9866–9875.
5. Pittenger, M. F.; Mackay, A. M.; Beck, S. C.; Jaiswal, R. K.; Douglas, R.; Mosca, J. D.; Moorman, M. A.; Simonetti, D. W.; Craig, S.; Marshak, D. R. Multilineage Potential of Adult Human Mesenchymal Stem Cells. *Science* **1999**, *284*, 143–147.
6. McBeath, R.; Pirone, D. M.; Nelson, C. M.; Bhadriraju, K.; Chen, C. S. Cell Shape, Cytoskeletal Tension, and Rhoa Regulate Stem Cell Lineage Commitment. *Dev. Cell* **2004**, *6*, 483–495.
7. Engler, A. J.; Sen, S.; Sweeney, H. L.; Discher, D. E. Matrix Elasticity Directs Stem Cell Lineage Specification. *Cell* **2006**, *126*, 677–689.
8. Kilian, K. A.; Bugarija, B.; Lahn, B. T.; Mrksich, M. Geometric Cues for Directing the Differentiation of Mesenchymal Stem Cells. *Proc. Natl. Acad. Sci. U.S.A.* **2010**, *107*, 4872–4877.
9. Yim, E. K.; Pang, S. W.; Leong, K. W. Synthetic Nanostructures Inducing Differentiation of Human Mesenchymal Stem Cells into Neuronal Lineage. *Exp. Cell Res.* **2007**, *313*, 1820–1829.
10. Dang, J. M.; Leong, K. W. Myogenic Induction of Aligned Mesenchymal Stem Cell Sheets by Culture on Thermally Responsive Electrospun Nanofibers. *Adv. Mater.* **2007**, *19*, 2775–2779.
11. Yim, E. K.; Darling, E. M.; Kulangara, K.; Guilak, F.; Leong, K. W. Nanotopography-Induced Changes in Focal Adhesions, Cytoskeletal Organization, and Mechanical Properties of Human Mesenchymal Stem Cells. *Biomaterials* **2010**, *31*, 1299–1306.
12. Burridge, K.; Fath, K.; Kelly, T.; Nuckolls, G.; Turner, C. Focal Adhesions: Transmembrane Junctions between the Extracellular Matrix and the Cytoskeleton. *Annu. Rev. Cell Biol.* **1988**, *4*, 487–525.
13. Watanabe, N.; Kato, T.; Fujita, A.; Ishizaki, T.; Narumiya, S. Cooperation between Mdia1 and Rock in Rho-Induced Actin Reorganization. *Nat. Cell Biol.* **1999**, *1*, 136–143.
14. Pirone, D. M.; Liu, W. F.; Ruiz, S. A.; Gao, L.; Raghavan, S.; Lemmon, C. A.; Romer, L. H.; Chen, C. S. An Inhibitory Role for Fak in Regulating Proliferation: A Link between Limited Adhesion and Rhoa-Rock Signaling. *J. Cell Biol.* **2006**, *174*, 277–288.
15. Andersson, A. S.; Backhed, F.; von Euler, A.; Richter-Dahlfors, A.; Sutherland, D.; Kasemo, B. Nanoscale Features Influence Epithelial Cell Morphology and Cytokine Production. *Biomaterials* **2003**, *24*, 3427–3436.
16. Santiago, J. A.; Pogemiller, R.; Ogle, B. M. Heterogeneous Differentiation of Human Mesenchymal Stem Cells in Response to Extended Culture in Extracellular Matrices. *Tissue Eng., Part A* **2009**, *15*, 3911–3922.
17. Slack-Davis, J. K.; Martin, K. H.; Tilghman, R. W.; Iwanicki, M.; Ung, E. J.; Autry, C.; Luzzio, M. J.; Cooper, B.; Kath, J. C.; Roberts, W. G.; *et al.* Cellular Characterization of a Novel Focal Adhesion Kinase Inhibitor. *J. Biol. Chem.* **2007**, *282*, 14845–14852.
18. Gabarra-Niecko, V.; Keely, P. J.; Schaller, M. D. Characterization of an Activated Mutant of Focal Adhesion Kinase: 'Superfak'. *Biochem. J.* **2002**, *365*, 591–603.
19. Teo, B. K.; Ankam, S.; Chan, L. Y.; Yim, E. K. Nanotopography/Mechanical Induction of Stem-Cell Differentiation. *Methods Cell Biol.* **2010**, *98*, 241–294.
20. Riveline, D.; Zamir, E.; Balaban, N. Q.; Schwarz, U. S.; Ishizaki, T.; Narumiya, S.; Kam, Z.; Geiger, B.; Bershadsky, A. D. Focal Contacts as Mechanosensors: Externally Applied Local Mechanical Force Induces Growth of Focal Contacts by an Mdia1-Dependent and Rock-Independent Mechanism. *J. Cell Biol.* **2001**, *153*, 1175–1186.
21. Qian, J.; Wang, J.; Lin, Y.; Gao, H. Lifetime and Strength of Periodic Bond Clusters between Elastic Media under Inclined Loading. *Biophys. J.* **2009**, *97*, 2438–2445.
22. Salasznyk, R. M.; Klees, R. F.; Hughlock, M. K.; Plopper, G. E. Erk Signaling Pathways Regulate the Osteogenic Differentiation of Human Mesenchymal Stem Cells on Collagen I and Vitronectin. *Cell Commun. Adhes.* **2004**, *11*, 137–153.
23. Liesi, P.; Laatikainen, T.; Wright, J. M. Biologically Active Sequence (Kdi) Mediates the Neurite Outgrowth Function of the Gamma-1 Chain of Laminin-1. *J. Neurosci. Res.* **2001**, *66*, 1047–1053.
24. Burridge, K.; Petch, L. A.; Romer, L. H. Signals from Focal Adhesions. *Curr. Biol.* **1992**, *2*, 537–539.
25. Li, W.; Lee, J.; Vikis, H. G.; Lee, S. H.; Liu, G.; Aurandt, J.; Shen, T. L.; Fearon, E. R.; Guan, J. L.; Han, M.; *et al.* Activation of Fak and Src Are Receptor-Proximal Events Required for Netrin Signaling. *Nat. Neurosci.* **2004**, *7*, 1213–1221.
26. Lawson, C.; Lim, S.-T.; Uryu, S.; Chen, X. L.; Calderwood, D. A.; Schlaepfer, D. D. Fak Promotes Recruitment of Talin to Nascent Adhesions to Control Cell Motility. *J. Cell Biol.* **2012**, *196*, 223–232.
27. Ilic, D.; Furuta, Y.; Kanazawa, S.; Takeda, N.; Sobue, K.; Nakatsuji, N.; Nomura, S.; Fujimoto, J.; Okada, M.; Yamamoto, T. Reduced Cell Motility and Enhanced Focal Adhesion Contact Formation in Cells from Fak-Deficient Mice. *Nature* **1995**, *377*, 539–544.
28. Rinnerthaler, G.; Geiger, B.; Small, J. V. Contact Formation During Fibroblast Locomotion: Involvement of Membrane Ruffles and Microtubules. *J. Cell Biol.* **1988**, *106*, 747–760.
29. Tilghman, R. W.; Slack-Davis, J. K.; Sergina, N.; Martin, K. H.; Iwanicki, M.; Hershey, E. D.; Beggs, H. E.; Reichardt, L. F.; Parsons, J. T. Focal Adhesion Kinase Is Required for the Spatial Organization of the Leading Edge in Migrating Cells. *J. Cell Sci.* **2005**, *118*, 2613–2623.
30. Lariviere, R. C.; Julien, J. P. Functions of Intermediate Filaments in Neuronal Development and Disease. *J. Neurobiol.* **2004**, *58*, 131–148.
31. Dupont, S.; Morsut, L.; Aragona, M.; Enzo, E.; Giulitti, S.; Cordenonsi, M.; Zanconato, F.; Le Digabel, J.; Forcato, M.; Bicciato, S.; *et al.* Role of Yap/Taz in Mechanotransduction. *Nature* **2011**, *474*, 179–183.
32. Tondreau, T.; Dejeneffe, M.; Meuleman, N.; Stamatopoulos, B.; Delforge, A.; Martiat, P.; Bron, D.; Lagneaux, L. Gene Expression Pattern of Functional Neuronal Cells Derived from Human Bone Marrow Mesenchymal Stromal Cells. *BMC Genomics* **2008**, *9*, 166.
33. Karel, Z. Contrast Limited Adaptive Histogram Equalization. In *Graphics Gems IV*; Heckbert, P. S., Ed.; Academic Press Professional, Inc.: Boston, MA, 1994; pp 474−485.
34. Bhadriraju, K.; Yang, M.; Alom Ruiz, S.; Pirone, D.; Tan, J.; Chen, C. S. Activation of Rock by Rhoa Is Regulated by Cell

Adhesion, Shape, and Cytoskeletal Tension. *Exp. Cell Res.* **2007**, *313*, 3616–3623.
35. Engel, E.; Martinez, E.; Mills, C. A.; Funes, M.; Planell, J. A.; Samitier, J. Mesenchymal Stem Cell Differentiation on Microstructured Poly (Methyl Methacrylate) Substrates. *Ann. Anat.* **2009**, *191*, 136–144.
36. Sakamoto, T.; Limouze, J.; Combs, C. A.; Straight, A. F.; Sellers, J. R. Blebbistatin, a Myosin II Inhibitor, Is Photoinactivated by Blue Light. *Biochemistry* **2005**, *44*, 584–588.